

# RELATIVISTIC PRECESSION FREQUENCIES OF RAPIDLY ROTATING COMPACT STARS

LEONARDO A. PACHÓN

Instituto de Física, Universidad de Antioquia, AA 1226 Medellín, Colombia

JORGE A. RUEDA

Dipartimento di Fisica and ICRA, Sapienza Università di Roma, P.le Aldo Moro 5, I-00185 Rome, Italy  
ICRANet, P.zza della Repubblica 10, I-65122 Pescara, Italy

AND

CÉSAR. A. VALENZUELA-TOLEDO

Departamento de Física, Universidad del Valle, A.A. 25360, Santiago de Cali, Colombia  
*Draft version March 14, 2019*

## ABSTRACT

We address the issue of the accuracy of the analytic exact solutions of the Einstein-Maxwell equations to describe the exterior spacetime of compact stars. As a test of accuracy, the radii of Innermost Stable Circular Orbits (ISCOs) as given by full numerical solutions of Einstein equations and by analytic exact exterior solutions, have been compared in the past. Here we propose an off-equatorial test of accuracy based on the comparison of the orbital frequencies of neutral test particles around compact objects. In particular, we compare the Keplerian frequency, the periastron and nodal precession frequencies, as well as the Lense-Thirring frequency, given by the Kerr solution and the six-parametric solution by Pachón, Rueda and Sanabria (2006). We evidenciate the major role of high-order multipole moments, e.g. the quadrupole and the current octupole moments, in the determination of the orbital frequencies, especially in the rapid rotation regime. The results of this work are relevant to cast a separatrix between Black Hole and Neutron Star signatures.

*Subject headings:* Exact solutions Einstein-Maxwell equations – Relativistic precession frequencies

## 1. INTRODUCTION

One of the greatest challenges of the general theory of relativity has been the construction of solutions to the Einstein-Maxwell field equations representing the gravitational field of compact stars, e.g. Neutron Stars (NSs). Stationary axially symmetric spacetimes satisfy basic properties one expects for rotating objects, namely time symmetry and reflection symmetry with respect to the rotation axis (see e.g. Pachón and Sanabria-Gómez 2006). The simplest stationary axially symmetric exact exterior vacuum solution describing a rotating configuration is the well-known Kerr metric (Kerr 1963). The Kerr metric is fully described by two free parameters: the mass  $M$  and the angular momentum  $J$  of the object. However, it is known from numerical models that the quadrupole moment of rotating neutron stars deviates considerably from the one given by the Kerr solution  $Q_{\text{Kerr}} = -J^2/(Mc^2)$  (see e.g. Laarakkers and Poisson 1999, for details).

In the mean time, a considerable number of analytic exterior solutions with a more complex multipolar structure than the one of the Kerr solution, has been developed (see e.g. Manko *et al.* 1995, 2000; Stephani *et al.* 2003). Whether analytic exterior solutions are accurate or not to describe the gravitational field of compact stars is an interesting and very active topic of research (see e.g. Stute and Camenzind 2002; Berti and Stergioulas 2004; Pachón *et al.* 2006, and references therein).

The accuracy of analytic solutions to describe the exterior geometry of a realistic rotating compact star has been tested

by comparing physical properties, e.g. the radius of the Innermost Stable Circular Orbit (ISCO) on the equatorial plane and the gravitational redshift (see Sibgatullin and Sunyaev 1998; Berti and Stergioulas 2004; Pachón *et al.* 2006, for details). In order to do such a comparison, the free parameters (i.e. the lowest multipole moments) of the analytic exterior spacetime, are fixed to the corresponding lowest multipole moments given by numerical interior solutions of the Einstein equations, for NS realistic models (see e.g. Berti and Stergioulas 2004).

Following such a procedure, the solution of Manko *et al.* (2000) has been compared by Stute and Camenzind (2002) and by Berti and Stergioulas (2004) with the numerical solutions for NSs calculated by Cook *et al.* (1994) and with those derived by Berti and Stergioulas (2004), respectively. However, being a generalization of the solution by Tomimatsu and Sato (1972), this specific solution cannot describe slowly rotating compact stars (see e.g. Berti and Stergioulas 2004), but the dynamics of astrophysical objects with anisotropic stresses (see Dubeibe *et al.* 2007, for details).

Following a similar procedure, based on tests of the ISCOs radii on the equatorial plane of the rotating neutron stars obtained by Berti and Stergioulas (2004), it has been shown that the six-parametric solution of Pachón *et al.* (2006) (hereafter PRS solution, see Sec. 2 for details) is more accurate than the model by Manko *et al.* (2000). In addition, being a generalization of the Kerr solution, this solution can be used for arbitrary rotation rates.

Besides the ISCOs radii, there are additional physical properties that can be computed with analytic and numerical models and thus useful to compare and contrast the accuracy of analytic exact models. The aim of this article is to analyze the

<sup>1</sup> leonardo.pachon@fisica.udea.edu.co

<sup>2</sup> jorge.rueda@icra.it

<sup>3</sup> cesar.valenzuela@correounivalle.edu.co

properties of orbital frequencies of neutral test particles in the PRS and in the Kerr geometries. In particular, we focus on the Keplerian frequency, the periastron and nodal precession frequencies, and the Lense-Thirring frequency.

The astrophysical relevance of these frequencies relies on the fact that they are often used to explain the Quasi-Periodic Oscillations (QPOs), observed e.g. in Low Mass X-ray Binaries (LMXBs). For instance, within the Relativistic Precession Model (RPM) introduced by [Stella and Vietri \(1998\)](#); [Morsink and Stella \(1999\)](#); [Stella et al. \(1999\)](#); [Stella and Vietri \(1999\)](#), the kHz QPOs are interpreted as a direct manifestation of the modes of relativistic epicyclic motion of blobs arising at various radii  $r$  in the inner parts of the accretion disk around the compact object, e.g. a Black Hole (BH) or a NS. The model identifies the so-called lower and upper (often called twin-peaks) kHz QPO frequencies with the periastron precession frequency  $\nu_p$  and the Keplerian frequency  $\nu_K$ .

Besides the RPM, the Keplerian  $\nu_K$  frequency, and the periastron  $\nu_p$  and nodal  $\nu_z$  precession frequencies, are involved in other QPO theoretical models (see e.g. [Lin et al. 2011](#), for a recent comparison of the existing models). Due to the influence of general relativistic effects in the determination of the epicyclic frequencies, an observational confirmation of any of the models might lead to an outstanding test of general relativity in the strong field regime. In this line, it is of interest to compare and contrast the orbital frequencies given by the Kerr solution and by the PRS solution (see Sec. 3), which help to establish the differences between possible BH and NS signatures. We emphasize in this article the major role of the quadrupole moment as well as of the octupole moment of the object, whose possible measurement can be used as a tool to test the no-hair theorem of BHs (see e.g. [Johannsen and Psaltis 2011](#)). In the case of NSs, the interpretation of QPOs as the manifestation of the epicyclic frequencies might lead to crucial information of the NS parameters e.g. its mass, angular momentum (see e.g. [Török et al. 2010](#)), as well as its quadrupole moment. These parameters, at the same time, reveal valuable information about the internal structure of the star, e.g. the equation of state (EOS).

The article is organized as follows. In Sec. 2 we recall the properties of the PRS solution. The computation of the orbital frequencies as well as the comparison of their features in the Kerr and in the PRS spacetimes, is shown in Sec. 3. In Sec. 4 we study the accuracy of the analytic formulas of the periastron and nodal frequencies derived by [Ryan \(1995\)](#) for stationary axially symmetric spacetimes. A discussion on possible additional effects to be accounted for in the determination of the orbital frequencies, e.g. the effect of magnetic dipole moment, are outlined in Sec. 5.

## 2. THE PRS ANALYTIC EXACT SOLUTION

We first recall the PRS analytic model ([Pachón et al. 2006](#)), for the exterior gravitational field of a compact object<sup>4</sup>. In the stationary axisymmetric case, the simplest form of the metric can be written as ([Papapetrou 1953](#))

$$ds^2 = -f(dt - \omega d\phi)^2 + f^{-1} [e^{2\gamma}(\rho^2 + dz^2) + \rho^2 d\phi^2], \quad (1)$$

where  $f$ ,  $\omega$  and  $\gamma$  are functions of the quasi-cylindrical Weyl coordinates  $(\rho, z)$ . Thus, the components of the metric tensor

$g_{\mu\nu}$  are

$$g_{\phi\phi} = \frac{\rho^2}{f(\rho, z)} - f(\rho, z)\omega(\rho, z)^2, \quad (2)$$

$$g_{tt} = -f(\rho, z), \quad (3)$$

$$g_{t\phi} = f(\rho, z)\omega(\rho, z), \quad (4)$$

$$g_{zz} = g_{\rho\rho} = \frac{e^{2\gamma(\rho, z)}}{f(\rho, z)} = \frac{1}{g^{zz}} = \frac{1}{g^{\rho\rho}}. \quad (5)$$

Using the above line element, the Einstein-Maxwell equations can be reformulated, via Ernst's procedure in terms of two complex potentials  $\mathcal{E}(\rho, z)$  and  $\Phi(\rho, z)$  ([Ernst 1968a,b](#)). By means of Sibgatullin's integral method ([Sibgatullin and Queen 1991](#); [Manko and Sibgatullin 1993](#)) this system of equations can be solved through

$$\mathcal{E}(z, \rho) = \int_{-1}^1 \frac{d\sigma}{\pi} \frac{e(\xi)\mu(\sigma)}{\sqrt{1-\sigma^2}}, \quad (6)$$

$$\Phi(z, \rho) = \int_{-1}^1 \frac{d\sigma}{\pi} \frac{f(\xi)\mu(\sigma)}{\sqrt{1-\sigma^2}}, \quad (7)$$

where  $e(z) := \mathcal{E}(z, \rho = 0)$  and  $f(z) := \Phi(z, \rho = 0)$ . The unknown function  $\mu(\sigma)$  must satisfy the singular integral equation

$$\oint_{-1}^1 \frac{\mu(\sigma)[e(\xi) + \bar{e}(\eta) + 2f(\xi)\bar{f}(\eta)]d\sigma}{(\sigma - \tau)\sqrt{1-\sigma^2}} = 0 \quad (8)$$

and the normalizing condition

$$\int_{-1}^1 \frac{\mu(\sigma)d\sigma}{\sqrt{1-\sigma^2}} = \pi, \quad (9)$$

where  $\xi = z + i\rho\sigma$ ,  $\eta = z + i\rho\tau$ ,  $\rho$  and  $z$  being the Weyl-Papapetrou quasi-cylindrical coordinates,  $\sigma, \tau \in [-1, 1]$ ,  $\bar{e}(\eta) := \overline{e(\bar{\eta})}$ ,  $\bar{f}(\eta) := \overline{f(\bar{\eta})}$  and the overbar stands for complex conjugation. In ([Pachón et al. 2006](#)), the Ernst potentials were chosen as

$$e(z) = \frac{z^3 - z^2(m + ia) - kz + is}{z^3 + z^2(m - ia) - kz + is}, \quad (10)$$

$$f(z) = \frac{qz^2 + i\mu z}{z^3 + z^2(m - ia) - kz + is}.$$

We calculate the multipole moments following the procedure of [Hoenselaers and Perjes \(1990\)](#). We denote the mass multipoles by  $M_i$  while, the current (rotation) multipoles, by  $S_i$ . The electric multipoles are denoted by  $Q_i$  and the magnetic ones by  $\mathcal{B}_i$ . Thus, for the PRS solution we have

$$M_0 = m, \quad M_2 = mk - ma^2, \quad \dots \quad (11)$$

$$S_1 = ma, \quad S_3 = -ma^3 + 2mak - ms, \quad \dots$$

$$Q_0 = q, \quad Q_2 = -a^2q - a\mu + kq, \quad \dots$$

$$\mathcal{B}_1 = \mu + aq, \quad \mathcal{B}_3 = -a^2\mu + \mu k - a^3q + 2akq - qs, \quad \dots \quad (12)$$

This allows us to identify  $m$  as the total mass,  $a$  as the total angular momentum per unit mass ( $a = J/m$ , being  $J$  the total angular momentum); while  $k$ ,  $s$  and  $\mu$  are associated to the mass-quadrupole moment  $M_2$ , current octupole  $S_3$  and magnetic dipole, respectively.

<sup>4</sup> Mathematica 8.0 scripts with the solution, some limiting cases as well as the calculations presented in this paper are available at <http://www.chem.utoronto.ca/~lpachon/scripts/nstars>

The potentials (10) can be written in an alternative way, we mean

$$e(z) = 1 + \sum_{i=3}^3 \frac{e_i}{z - \beta_i}, \quad f(z) = \sum_{i=3}^3 \frac{f_i}{z - \beta_i}, \quad (13)$$

with

$$e_j = (-1)^j \frac{2m\beta_j^2}{(\beta_j - \beta_k)(\beta_j - \beta_i)}, \quad (14)$$

$$f_j = (-1)^{j+1} \frac{i\mu + d\beta_j}{(\beta_j - \beta_k)(\beta_j - \beta_i)}, \quad i, k \neq j. \quad (15)$$

Then, using Eqs. (6) and (10), we obtain the Ernst potentials

$$\mathcal{E} = \frac{A+B}{A-B}, \quad \Phi = \frac{C}{A-B}, \quad (16)$$

and the metric functions in the whole spacetime

$$f = \frac{A\bar{A} - B\bar{B} + C\bar{C}}{(A-B)(\bar{A}-\bar{B})}, \quad e^{2\gamma} = \frac{A\bar{A} - B\bar{B} + C\bar{C}}{K\bar{K} \prod_{n=1}^6 r_n}, \quad (17)$$

$$\omega = \frac{\text{Im}[(A+B)\bar{H} - (\bar{A}+\bar{B})G - C\bar{I}]}{A\bar{A} - B\bar{B} + C\bar{C}}, \quad (18)$$

where the functions  $A$ ,  $B$ ,  $C$ ,  $H$ ,  $G$ ,  $K$ , and  $I$  can be found in the Appendix A.

The PRS electrovacuum exact solution belongs to the extended  $N$ -soliton solution of the Einstein-Maxwell equations derived by Ruiz *et al.* (1995), in the particular case  $N = 3$ . In addition, the functional form of the metric functions resembles the one derived previously by Bretón *et al.* (1999). Besides the limiting cases discussed in Pachón *et al.* (2006), it is worth mentioning that in the vacuum case,  $q = 0$  and  $\mu = 0$ , for non arbitrary differential rotation,  $s = 0$ , this solution reduces to (Manko *et al.* 1995) under the same physical conditions, i.e.  $q = 0$ ,  $c = 0$  and  $b = 0$  in Manko *et al.* (1995).

### 3. ORBITAL MOTION FREQUENCIES

Although for the case of stars, contributions from the magnetic field could be relevant (see e.g. Bakala *et al.* 2010; Sanabria-Gómez *et al.* 2010), we focus in this work on the frequencies of neutral particles orbiting a neutral compact object. We study here the Keplerian frequency, the periastron and nodal precession frequencies, and the dragging of inertial frames (Lense-Thirring) frequency.

The geodesic motion along the radial coordinate of test particles is governed by the effective potential

$$V(\rho) = 1 - \frac{E^2 g_{\phi\phi} + 2ELg_{t\phi} + L^2 g_{tt}}{g_{t\phi}^2 - g_{tt}g_{\phi\phi}}, \quad (19)$$

where, for circular orbits, the energy  $E$  and angular momentum  $L$  are determined by the conditions  $V = 0$  and  $dV/d\rho = 0$  (see Eqs. 22–23). The frequencies at the ISCO's location (determined by the additional condition  $d^2V/d\rho^2 = 0$ ) are of particular interest. Thus, before starting the discussion of the frequencies, it is important to explore the ISCO parametric dependence. In the upper panel of Fig. 1, we have plotted contours of constant ISCO radii as a function of the star angular-momentum per unit mass  $J/M_0 = a$  and the star

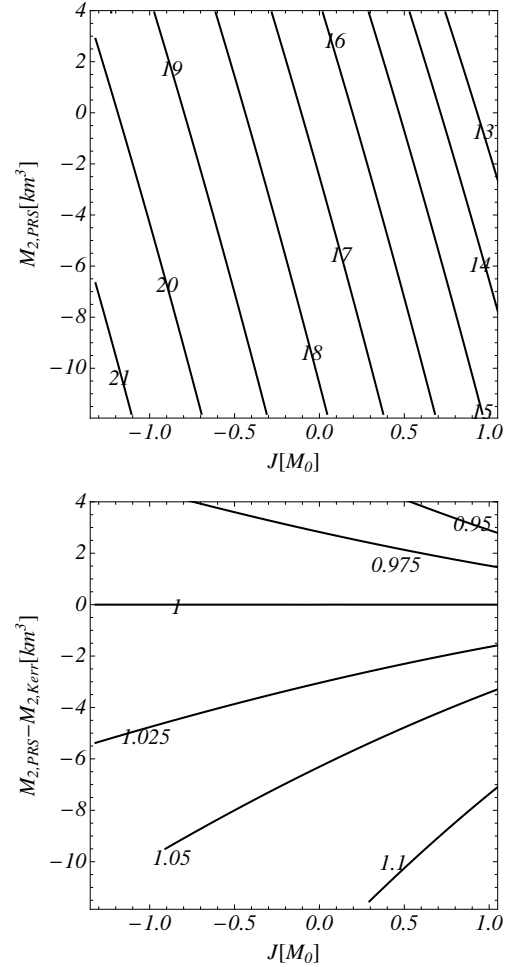


FIG. 1.— Upper panel: Contours of constant ISCO radius as a function of the star angular momentum per unit mass  $J/M_0$  and the quadrupole moment  $M_2$ . Contours are labeled by the corresponding value of the ISCO radius in km. Lower panel: Contours of constant ratio  $r_{\text{ISCO,PRS}}/r_{\text{ISCO,Kerr}}$  as a function of  $J/M_0$  and the difference  $M_{2,\text{PRS}} - M_{2,\text{Kerr}}$ . Negative values of  $J$  depict the counter-rotating case and negative values of  $M_2$  correspond to the oblate case.

quadrupole moment  $M_2$ . The influence of the quadrupole moment can be evidenced by the fact that the contour lines deviate from vertical lines. We can see that the ISCO radius decreases for increasing  $J$  and decreasing  $M_2$ . In the lower panel, we have plotted contours of constant value for the ratio  $r_{\text{ISCO,PRS}}/r_{\text{ISCO,Kerr}}$  as a function of  $J/M_0$  and the difference between  $M_{2,\text{PRS}}$  and the Kerr quadrupole  $M_{2,\text{Kerr}} = -ma^2$ , i.e.  $M_{2,\text{PRS}} + ma^2$ , see Eq. (11). Deviations from the Kerr geometry are evident.

It is worth noticing that, for the case of *realistic models* of NS's, the ISCO radius obtained using the PRS solution was already confronted to other models (see Pachón *et al.* 2006, for details) and the accuracy of the PRS solution was shown to be superior in all cases. Negative values of the angular momentum correspond to the radii of the counter-rotating orbits obtained here through the change  $g_{t\phi} \rightarrow -g_{t\phi}$  (see discussion below). In Figs. 1–5, we have fixed as an example  $M_0 = m = 1.88M_\odot$  and  $s = 0$ .

#### 3.1. Keplerian frequency

Now we turn into the frequencies analysis. For stationary axially symmetric spacetimes, the frequency of Keplerian or-

bits is given by (see e.g. Ryan 1995)

$$\Omega_K = \frac{-g_{t\phi, \rho} \pm \sqrt{g_{t\phi, \rho}^2 - g_{\phi\phi, \rho} g_{tt, \rho}}}{g_{\phi\phi, \rho}}, \quad (20)$$

where a colon stands for partial derivative with respect to the indicated coordinate and ‘+’ and ‘-’ stands for corotating and counter-rotating orbits, respectively.

For the case of static spacetimes, i.e. for  $\omega = 0$  and therefore  $g_{t\phi} = 0$ ,  $\Omega_K = \pm \sqrt{-g_{\phi\phi, \rho} g_{tt, \rho}} / g_{\phi\phi, \rho}$  and the energy  $E$  and angular momentum  $L$  per mass  $\mu$  of the test particle can be expressed in terms of the metric tensor components (see e.g. Ryan 1995),

$$\frac{E}{\mu} = \frac{-g_{tt}}{\sqrt{-g_{tt} - g_{\phi\phi} \Omega_K^2}}, \quad \frac{L}{\mu} = \frac{g_{\phi\phi} \Omega_K}{\sqrt{-g_{tt} - g_{\phi\phi} \Omega_K^2}}. \quad (21)$$

From here, it is clear that taking the negative branch of the root for  $\Omega_K$  in Eq. (20) is equivalent to studying a particle with opposite angular momentum, i.e.  $L_{\text{count-rot}} = -L_{\text{co-rot}}$ . Thus, in the static case the magnitude of the energy and angular momentum are invariant under the change  $\Omega_K \rightarrow -\Omega_K$ .

Now we consider the case of stationary space times,  $\omega \neq 0$ . The energy  $E$  and angular momentum  $L$  per mass  $\mu$  are, in this case, given by (see e.g. Ryan 1995)

$$\frac{E}{\mu} = \frac{-g_{tt} - g_{t\phi} \Omega_K}{\sqrt{-g_{tt} - 2g_{t\phi} \Omega_K - g_{\phi\phi} \Omega_K^2}}, \quad (22)$$

$$\frac{L}{\mu} = \frac{g_{t\phi} + g_{\phi\phi} \Omega_K}{\sqrt{-g_{tt} - 2g_{t\phi} \Omega_K - g_{\phi\phi} \Omega_K^2}}. \quad (23)$$

The counter-rotating condition expressed by the negative branch of Eq. (20), can be generated by the change  $g_{t\phi} \rightarrow -g_{t\phi}$ , which seems to be a more physical and transparent condition. In contrast to the static case, the counter-rotating orbit has now different energy and different magnitude of the angular momentum due the presence of the dragging of the inertial frames, characterized by the metric component  $g_{t\phi}$  (cf. Eq. (26) below). In a nutshell, the dynamics of counter-rotating orbits of a test-particle can be derived, starting from the positive branch of Eq. (20), by considering a spacetime with  $g_{t\phi} \rightarrow -g_{t\phi}$ .

For the vacuum case, a similar analysis as the one developed by Herrera *et al.* (2006), clearly show that the change in the global sign of  $g_{t\phi}$  is achieved by changing not only the angular momentum,  $J \rightarrow -J$ , of the star, but *all the rotational multipolar moments*. For the Kerr metric this change is obtained by changing the sign of the parameter  $a$  (see Appendix B) while in the PRS solution we need additionally change the sign of the parameter  $s$  associated to differential rotation, i.e., by changing  $a \rightarrow -a$  and  $s \rightarrow -s$ .<sup>5</sup>

Once we have clarified this important issue about the corotating and counter-rotating orbits, we proceed to analyze the functional dependence of the Keplerian frequency on the multipole moments. In the upper panel of Fig. 2, we have plotted contours of constant Keplerian frequency,  $\nu_K = \Omega_K / (2\pi)$ , as a function of the star angular-momentum per unit mass  $J/M_0$

<sup>5</sup> For the vacuum case, in the solution by Manko *et al.* (2000), the sign change of  $g_{t\phi}$  is obtained after performing the replacements  $a \rightarrow -a$  and  $b \rightarrow -b$ .

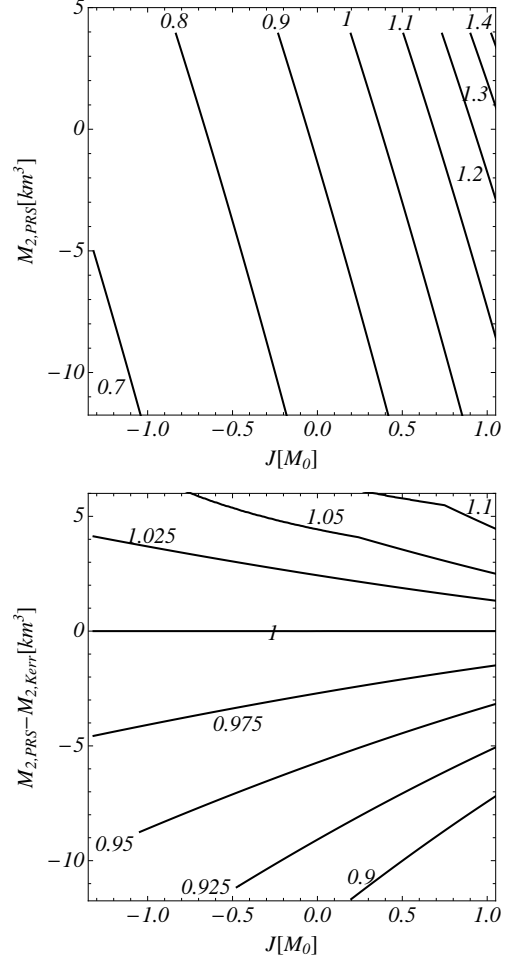


FIG. 2.— Upper panel: Contours of constant  $\nu_K = \Omega_K / (2\pi)$  as a function of the angular momentum per unit mass  $J/M_0$  and quadrupole moment  $M_2$ . Contours are labeled by the corresponding value of  $\nu_K$ , in kHz. Lower panel: Contours of constant ratio  $\nu_{K, \text{PRS}} / \nu_{K, \text{Kerr}}$  as a function of  $J$  and the difference  $M_{2, \text{PRS}} - M_{2, \text{Kerr}}$ .

and the quadrupole moment  $M_2$ . It can be seen that the influence of the quadrupole moment is non-negligible, as evidenced from the departure of the contour lines from vertical lines. The Keplerian frequency grows for increasing  $J$  and  $M_2$  increasing. In the lower panel, we have plotted contours of constant value for the ratio  $\nu_{K, \text{PRS}} / \nu_{K, \text{Kerr}}$  as a function of  $J/M_0$  and the difference between the quadrupole moment of the PRS solution  $M_{2, \text{PRS}}$  and the Kerr quadrupole  $M_{2, \text{Kerr}}$ .

### 3.2. Periastron Precession and Nodal Frequencies

The epicyclic frequencies are the precession frequencies of the periastron and of the orbital plane of circular orbit, slightly perturbed in the radial and in the vertical directions, respectively. According to Ryan (1995), they can be obtained from

$$\Omega_\alpha = \Omega_K - \left\{ -\frac{g^{\alpha\alpha}}{2} \left[ (g_{tt} + g_{t\phi} \Omega)^2 \left( \frac{g_{\phi\phi}}{\rho^2} \right)_{, \alpha\alpha} - 2(g_{tt} + g_{t\phi} \Omega)(g_{t\phi} + g_{\phi\phi} \Omega) \left( \frac{g_{t\phi}}{\rho^2} \right)_{, \alpha\alpha} + (g_{t\phi} + g_{\phi\phi} \Omega)^2 \left( \frac{g_{tt}}{\rho^2} \right)_{, \alpha\alpha} \right] \right\}^{1/2}, \quad (24)$$

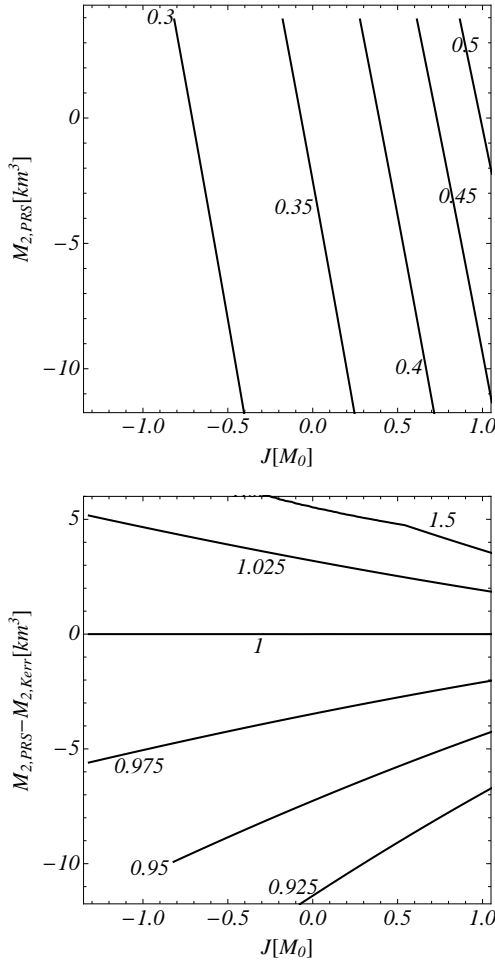


FIG. 3.— Upper panel:  $\nu_K - \nu_\rho$  as a function of the the angular momentum  $J$  and quadruple moment  $M_2$ . Contours are labeled by the corresponding value of  $\nu_K - \nu_\rho$ , in kHz. Lower panel: Contours of constant ratio  $(\nu_{K,PRS} - \nu_{\rho,PRS})/(\nu_{K,Kerr} - \nu_{\rho,Kerr})$  as a function of  $J$  and the difference  $M_{2,PRS} - M_{2,Kerr}$ .

where  $\alpha = \{\rho, z\}$ .

$$\Omega_\alpha = \Omega_K - \left\{ -\frac{g^{\alpha\alpha}}{2} \left[ g_{tt}^2 \left( \frac{g_{\phi\phi}}{\rho^2} \right)_{,\alpha\alpha} - 2g_{tt}g_{\phi\phi}\Omega \left( \frac{1}{\rho^2} \right)_{,\alpha\alpha} + (g_{\phi\phi}\Omega)^2 \left( \frac{g_{tt}}{\rho^2} \right)_{,\alpha\alpha} \right] \right\}^{1/2}, \quad (25)$$

In the upper panels of Figs. 3-4, we have plotted contours of constant periastron precession  $\nu_K - \nu_\rho$  and nodal frequencies  $\nu_K - \nu_z$ , as functions of  $J/M_0$  and  $M_2$ , where  $\nu_\rho = \Omega_\rho/(2\pi)$  and  $\nu_z = \Omega_z/(2\pi)$ . We can see now that influence of the quadrupole moment is quite important. The periastron precession and the nodal frequency increase for increasing  $J$  and decreasing  $M_2$ , at fixed  $M_0$ . In the lower panels we have plotted contours of constant ratio  $(\nu_{K,PRS} - \nu_{\rho,PRS})/(\nu_{K,Kerr} - \nu_{\rho,Kerr})$  and  $(\nu_{K,PRS} - \nu_{z,PRS})/(\nu_{K,Kerr} - \nu_{z,Kerr})$  as a function of  $J/M_0$  and the difference  $M_{2,PRS} - M_{2,Kerr}$ , in order to evidentiate deviations from the Kerr solution.

### 3.3. Dragging of Inertial Frames

The influence of general relativistic effects like Lense-Thirring precession in the dynamics of neutron stars has been

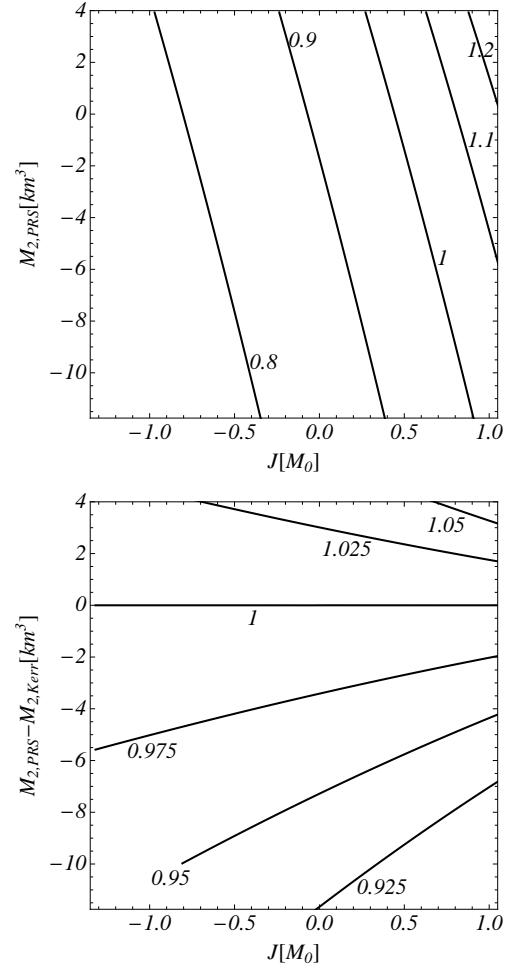


FIG. 4.— Upper panel: Contours of constant  $\nu_K - \nu_z$  as a function of  $J/M_0$  and the quadruple moment  $M_2$ . Here  $\nu_z = \Omega_z/(2\pi)$ . Contours are labeled by the corresponding value of  $\nu_K - \nu_z$ , in kHz. Lower panel: Contours of constant ratio  $(\nu_{K,PRS} - \nu_{z,PRS})/(\nu_{K,Kerr} - \nu_{z,Kerr})$  as a function of  $J/M_0$  and the difference  $M_{2,PRS} - M_{2,Kerr}$ .

studied by Stella and Vietri (1998) and Morsink and Stella (1999) and very recently around the Earth gravitational field as a test for general relativity by Lucchesi and Peron (2010).

In our case, the Lense-Thirring frequency is given by (Ryan 1995)

$$\omega_{LT} = -\frac{g_{t\phi}}{g_{\phi\phi}}. \quad (26)$$

As it was noted by Stella and Vietri (1998), the precession frequency due to the frame-dragging effect has approximately the right magnitude and radial dependence to explain observations of accreting neutron stars made by the Rossi X-Ray Timing Explorer satellite. If this interpretation is confirmed, it would provide a confirmation of the Lense-Thirring effect that includes its radial dependence, a test that is beyond reach of any other current or planned experiment to test frame dragging (see Morsink and Stella 1999, for details).

In Fig. 5, we have plotted contours of equal frame dragging frequency  $\nu_{LT} = \Omega_{LT}/(2\pi)$ , as function of the star angular-momentum and the star quadrupole momentum, at fixed mass  $M_0$ . Analogously to the case of the periastron precession and nodal frequencies, the influence of the quadrupole moment is very strong. It is worth mentioning that frame dragging precession can be affected as well by strong electromagnetic

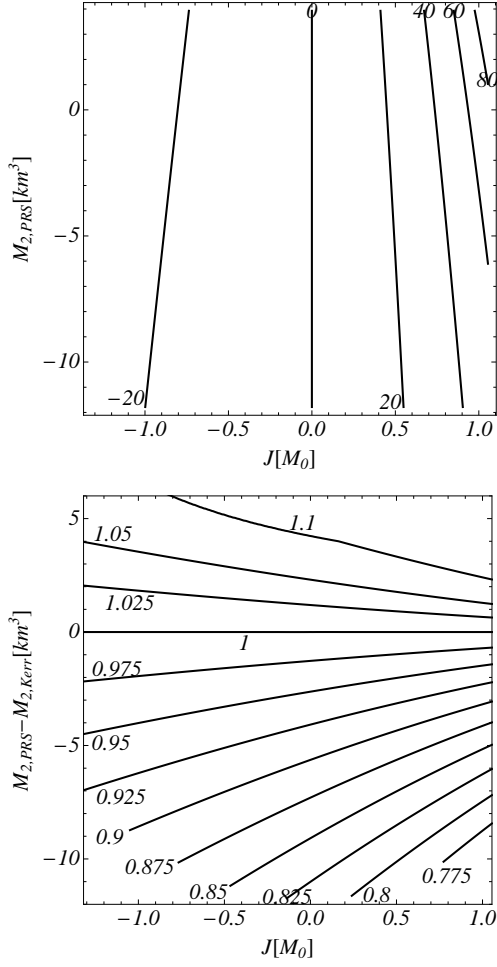


FIG. 5.— Upper panel: Contours of constant  $\nu_{LT} = \Omega_{LT}/(2\pi)$  as a function of the angular momentum per unit mass  $J/M_0$  and the quadrupole moment  $M_2$ . Contours are labeled by the corresponding value of  $\nu_{LT}$ , in Hz. Lower panel: Contours of constant ratio  $\nu_{LT,PRS}/\nu_{LT,Kerr}$  as a function of  $J/M_0$  and the difference  $M_2, PRS - M_2, Kerr$ .

fields [Herrera et al. \(2006\)](#) and further research in this respect deserve the due attention.

### 3.4. Kerr vs. PRS Frequencies

The above frequencies have been extensively studied in literature for uniformly rotating NSs (see e.g. [Stella and Vietri 1998](#); [Morsink and Stella 1999](#); [Sibgatullin 2002](#); [Stergioulas 2003](#); [Haensel et al. 2009](#)) while, up to the best of our knowledge, there is no available data for the frequencies of realistic NS models with differential rotation. It is thus interesting to investigate the effects of differential rotation from the theoretical point of view by analyzing both the case  $s = 0$  (or equivalently  $b = 0$  in the solution by [Manko et al. \(1995\)](#)) as well as  $s \neq 0$  of the PRS solution.

In Figs. 6–9, we plot the  $\nu_K - \nu_\rho$  vs.  $\nu_K$  diagram, relevant e.g. for the relativistic precession model of QPOs ([Stella and Vietri 1998](#); [Morsink and Stella 1999](#); [Stella et al. 1999](#); [Stella and Vietri 1999](#)), for the Kerr and the PRS solutions. In particular, we discuss here the NS models studied by [Morsink and Stella \(1999\)](#), for the L EOS. In the case  $s \neq 0$  we fix the parameter  $s$  in such a way that the radius of the corotating ISCO of the analytical solution  $R_{ISCO,PRS}$  matches the value predicted by the numerical solution for  $R_{ISCO}$ . The highly non-linear dependence of  $R_{ISCO,PRS}$  on the parameter  $s$

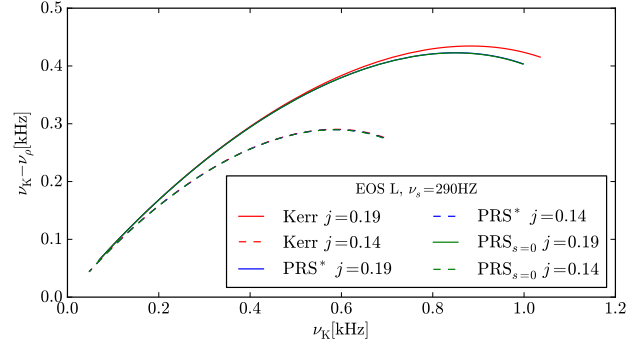


FIG. 6.— Periastron versus Keplerian frequency as given by the Kerr and the PRS analytic solutions. The lowest multipole moments has been fixed from the numerical models of rotating NSs of ([Morsink and Stella 1999](#)), for the L EOS. The rotation frequency of the NS is  $\nu_s = \Omega/(2\pi)$ , where  $\Omega$  is the angular velocity of the star, and  $j = J/m^2$  is the dimensionless angular momentum parameter. The corresponding masses of the configurations with  $j = \{0.14, 0.19\}$  are  $m = \{2.71, 1.88\}M_\odot$  while the  $k$ -parameter values are  $\{-1.14, -0.24\}$ , respectively. The  $s$ -parameter values for  $PRS^*$  are  $s = \{0.29995, 1.2555\}$  for  $j = \{0.19, 0.14\}$ , respectively.

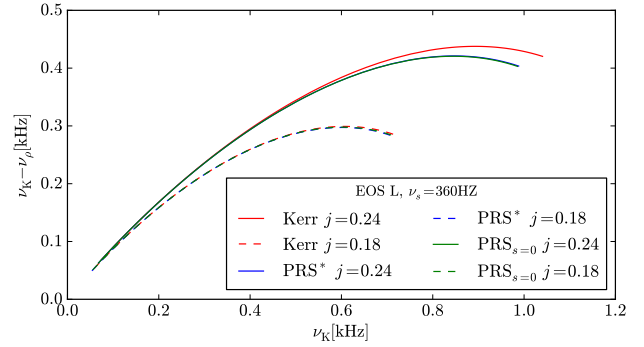


FIG. 7.— Periastron versus Keplerian frequency as given by the Kerr and the PRS analytic solutions. The lowest multipole moments has been fixed from the numerical models of rotating NSs of ([Morsink and Stella 1999](#)), for the L EOS. The rotation frequency of the NS is  $\nu_s = \Omega/(2\pi)$ . The corresponding masses of the configurations with  $j = \{0.18, 0.24\}$  are  $m = \{2.71, 1.94\}M_\odot$  while the  $k$ -parameter values are  $\{-1.65, -0.37\}$ , respectively. The  $s$ -parameter values for  $PRS^*$  are  $s = \{0.6905, -2.3045\}$  for  $j = \{0.24, 0.18\}$ , respectively.

makes the equation  $R_{ISCO,PRS} - R_{ISCO} = 0$  to have different solutions. In our simulations we choose for  $|s|$  the smallest root, with a numerical accuracy of  $10^{-6}$  km.

From Figs. 6–9, it is evident that deviations from the Kerr’s solution, for *realistic models of NSs*, are present because of the influence of the deformation of the star as well as, although in less proportion, by the octupole current. In general, we observe that the larger the angular momentum, the poorer the performance of the predictions by Kerr’s solution. The minor influence, in this case, of the current octupole is expected from the small values of the parameter  $s$  needed to fit the ISCO radius. The effect of this parameter is only appreciable in Fig. 9, by the separation of the curves blue and green. Of course, larger values of  $s$  will enhance as well deviations from the Kerr spacetime.

## 4. ACCURACY OF RYAN’S ANALYTIC FORMULAS

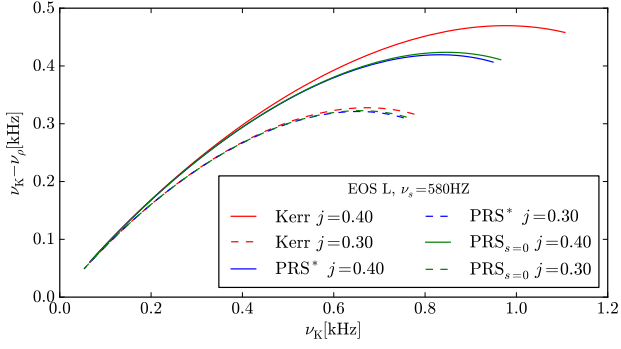


FIG. 8.— Periastron versus Keplerian frequency as given by the Kerr and the PRS analytic solutions. The lowest multipole moments has been fixed from the numerical models of rotating NSs of (Morsink and Stella 1999), for the L EOS. The rotation frequency of the NS is  $\nu_s = \Omega/(2\pi)$ . The corresponding masses of the configurations with  $j = \{0.3, 0.4\}$  are  $m = \{2.72, 2.07\}M_\odot$  while the  $k$ -parameter values are  $\{-4.11, -1.11\}$ , respectively. The  $s$ -parameter values for PRS\* are  $s = \{-5.6956, -4.7915\}$  for  $j = \{0.40, 0.30\}$ , respectively.

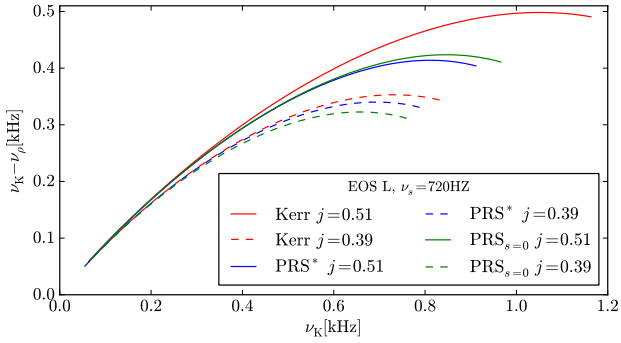


FIG. 9.— Periastron versus Keplerian frequency as given by the Kerr and the PRS analytic solutions. The lowest multipole moments has been fixed from the numerical models of rotating NSs of (Morsink and Stella 1999), for the L EOS. The rotation frequency of the NS is  $\nu_s = \Omega/(2\pi)$ . The corresponding masses of the configurations with  $j = \{0.39, 0.51\}$  are  $m = \{2.73, 2.00\}M_\odot$  while the  $k$ -parameter values are  $\{-6.44, -2.05\}$ , respectively. The  $s$ -parameter values for PRS\* are  $s = \{-12.888, -4.424\}$  for  $j = \{0.51, 0.39\}$ , respectively.

Following a series expansion procedure in powers of  $1/\rho$ , Ryan (1995) found that the periastron and nodal precession frequencies,  $\Omega_\rho$  and  $\Omega_z$  given by Eq. (25), can be written as a function of the Keplerian frequency as

$$\begin{aligned} \frac{\Omega_\rho}{\Omega_K} &= 3\mathcal{V}^2 - 4\frac{S_1}{M_0^2}\mathcal{V}^3 + \left(\frac{9}{2} - \frac{3M_2}{2M_0^3}\right)\mathcal{V}^4 - 10\frac{S_1}{M_0^2}\mathcal{V}^5 \\ &+ \left(\frac{27}{2} - 2\frac{S_1^2}{M_0^4} - \frac{21M_2}{2M_0^3}\right)\mathcal{V}^6 + \left(-48\frac{S_1}{M_0^2} - 5\frac{S_1M_2}{M_0^5}\right. \\ &+ 9\frac{S_3}{M_0^4}\mathcal{V}^7 + \left(\frac{405}{8} + \frac{2243S_1^2}{84M_0^4} - \frac{661M_2}{14M_0^3}\right. \\ &\left. - \frac{21M_2^2}{8M_0^6} + \frac{15M_4}{4M_0^5}\right)\mathcal{V}^8 + \dots, \end{aligned} \quad (27)$$

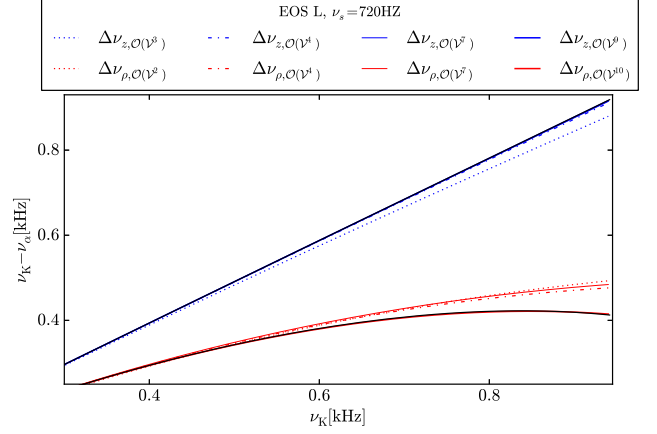


FIG. 10.— Comparison of the  $\Delta\nu_z = \nu_K - \nu_z$  and  $\Delta\nu_\rho = \nu_K - \nu_\rho$  frequencies given by PRS solution with  $s = 0$  and by the approximate expressions (27-28) derived by Ryan (1995) for realistic NSs models (Morsink and Stella 1999). Parameters as in Fig. 9.

and

$$\begin{aligned} \frac{\Omega_z}{\Omega_K} &= 2\frac{S_1}{M_0^2}\mathcal{V}^3 + \frac{3M_2}{2M_0^3}\mathcal{V}^4 + \left(7\frac{S_1^2}{M_0^4} + 3\frac{M_2}{M_0^3}\right)\mathcal{V}^6 \\ &+ \left(11\frac{S_1M_2}{M_0^5} - 6\frac{S_3}{M_0^4}\right)\mathcal{V}^7 + \left(\frac{153S_1^2}{28M_0^4} + \frac{153M_2}{28M_0^3}\right. \\ &\left. + \frac{39M_2^2}{8M_0^6} - \frac{15M_4}{4M_0^5}\right)\mathcal{V}^8 + \dots, \end{aligned} \quad (28)$$

where  $\mathcal{V} = (M_0\Omega_K)^{1/3}$ ,  $[M_0, M_2, M_4]$  are the lowest three mass moments and,  $[S_1, S_3]$ , are the lowest two current moments. For the present vacuum case,  $M_4 = m(a^4 - 3a^2 + k^2 + 2as)$ .

The above approximate formulas show that the higher multipole moments become important at high frequencies. From the first term of these expansions, it follows the relations

$$\nu_K = 3^{-3/5}(2\pi)^{-2/5}m^{-2/5}\nu_\rho^{3/5}, \quad (29)$$

$$\nu_z = (2/3)^{6/5}\pi^{1/5}j m^{1/5}\nu_\rho^{6/5}, \quad (30)$$

corresponding to the weak field slow rotation limit. These formulas have been shown to be qualitatively consistent with data from low frequency QPOs observed in some LMXBs involving old accreting NSs (see e.g. Stella et al. 1999, for details).

At high frequencies, e.g. of the order of kHz, deviations from the above scaling laws are appreciable. In Figs. 10 and 11 we compare the  $\nu_\rho - \nu_K$  and the  $\nu_K - \nu_z$  vs.  $\nu_K$  and  $\nu_K - \nu_\rho$  vs.  $\nu_K$  relations as given by the full expressions (25) and by the approximate formulas (27) and (28), respectively. Results are presented for the cases  $s = 0$  (see Fig. 10) and for the case when  $s$  is fixed to match the ISCO radius derived by Morsink and Stella (1999) (see Fig. 11). Since the most interesting case for this comparison is the fast rotating case presented in Fig. 9, in Figs. 10 and 11 we analyze this case. The Keplerian frequency used in (27) and (28) was calculated using the PRS solution with either  $s = 0$  or  $s$  fixed.

In Fig. 10 we plot  $\Delta\nu_z = \nu_K - \nu_z$  using PRS<sub>s=0</sub> and the contribution from different multipole moments from Eq. (27). The blue dotted curve depicts the contribution from the angular momentum (we cut the series in (28) after  $\mathcal{V}^3$ ), for the blue dot-dashed curve we add the first contribution from the quadrupole moment  $M_2$  (we cut the series after  $\mathcal{V}^4$ ), for the

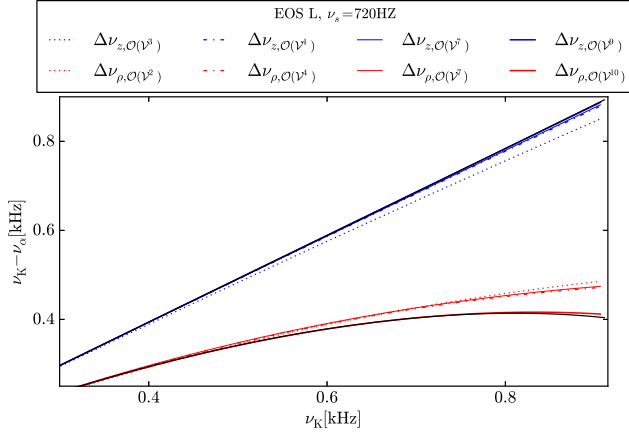


FIG. 11.— Comparison of the  $\Delta\nu_z = \nu_K - \nu_z$  and  $\Delta\nu_\rho = \nu_K - \nu_\rho$  frequencies given by PRS solution for fixed  $s$  and by the approximate expressions (27-28) derived by Ryan (1995), for realistic NSs models (Morsink and Stella 1999). Parameters as in Fig. 9.

thin blue line we now add the first contribution from the octupole mass-current (we cut the series after  $\mathcal{V}^7$ ) and finally in the thick blue line we consider contributions for higher multipole moments and stop the series after  $\mathcal{V}^9$  (not shown in (28)). For this case, we can see that Ryan’s expressions clearly tend, from the bottom, to the exact result (continuous black curve) obtained by using the PRS solution. In Fig. 11, we have the same situation but using the PRS with  $s$  fixed, here a tiny deviation from the contribution up  $\mathcal{V}^7$  can be appreciated. In general, Eq. (27) fits very well the exact result.

In Fig. 11 we plot  $\Delta\nu_\rho = \nu_K - \nu_\rho$  using  $\text{PRS}_{s=0}$  and the contribution from different multipole moments from Eq. (28) following the same procedures as decried above. In this case, the Ryan’s expressions tend from the top to the exact result (continuous black curve). It is interesting to see that the introduction of the octupole moment (thin red line) makes the approximation to deviate from the exact result, however by including more terms the accuracy is enhanced. In Fig. 11, we have the same situation but using the PRS with  $s$  fixed, this time deviations from the contribution up  $\mathcal{V}^7$  can be clearly appreciated and higher order terms of  $\mathcal{V}$  are needed. In general, Eq. (27) fits perfectly when taking up  $\mathcal{V}^{10}$  in the expansion.

So, the importance of the high-order multipole moments e.g. the quadrupole as well as the octupole moment, is evident in the high-frequency regime. This is in line with the results shown in Figs. 2-4 and in Figs. 6-9. Since the fit taking up order  $\mathcal{V}^{10}$  is excellent, for future works taking (27) and (28) up to this order will be enough.

## 5. CONCLUDING REMARKS

We have studied in this article the orbital motion of neutral test particles in the PRS and Kerr spacetime geometries. In particular we have emphasized on the Keplerian frequency, the periastron precession and nodal frequencies, and the Lense-Thirring frequency. The differences of the properties of the precession frequencies as given by the PRS and the Kerr solution have been outlined in detail, see e.g. Figs. 2-4 and Figs. 6-9. The epicyclic frequencies of the Kerr solution deviate considerably from the ones given by the PRS solution, especially in the rapid  $\sim$ kHz rotation regime, see Figs. 6-9. Such differences appear as a direct manifestation of the influence of the high order e.g. quadrupole and octupole multipole moments, see Figs. 2-4 and Figs. 10-11.

The above results are useful to distinguish the signatures of BH and NS, relevant to establish a separatrix for the identification of the compact objects e.g. in LMXBs. Consequently, these results might become important for testing the no-hair theorem of BHs (see e.g. Johannsen and Psaltis 2011). Equally important, the application of the epicyclic frequencies to the explanation of QPOs in LMXBs possessing a NS, can unveil information on the NS parameters, leading to a possible identification of the behavior of the nuclear matter EOS at supranuclear densities.

The generalization of the present work to the electrovacuum case is important to establish the influence of the magnetic dipole and quadrupole moments on the orbital motion of particles around compact objects (see e.g. Bakala et al. 2010; Sanabria-Gómez et al. 2010). Interesting effects on the epicyclic frequencies due to the presence of the magnetic dipole have been already pointed out recently by Bakala et al. (2010), although neglecting rotation and the contribution of the electromagnetic field to the curvature. In that work the authors assume the model of the star as a dipole magnetic field superimposed on a Schwarzschild black hole. The effects of the magnetic dipole on the location of the ISCO, within the PRS solution, has been investigated by Sanabria-Gómez et al. (2010).

A complete analysis of the effects due to the emergence of electromagnetic structure on the orbital motion of charged particles is therefore of interest and deserve the appropriate attention. Recent observations have shown that for stars with strong magnetic fields the quadrupole and octupole magnetic terms make significant contributions to the magnetic field (Donati et al. 2006), which indicates that arbitrary higher order multipole components might be required in a realistic model. The presence of a magnetic quadrupole demands the breaking of the reflection symmetry (see Pachón and Sanabria-Gómez 2006, for details), by means of a slightly change to the Ernst electric potential over the symmetry axis

$$f(z) = \frac{qz^2 + i\mu z + i\zeta}{z^3 + z^2(m - ia) - kz + is}, \quad (31)$$

a quadrupolar magnetic component  $\mathcal{B}_2 = \zeta$  can be introduced to the PRS solution. Such a change generates just a redefinition of the coefficients  $f_i$  in Eq. (15). In this way the PRS solution can be readily use to explore the effect of strong magnetic fields with non-dipolar structure.

The authors thank Emmanuel Berti for directing our attention to the astrophysical relevance of the periastron precession and nodal frequencies. This work was partially supported by Fundación para la Promoción de la Investigación y la Tecnología del Banco la República grant number 2879. L.A.P. acknowledges the financial support by the Colombian Institute for the Science and Technology Development (COLCIENCIAS), and from Comité para el Desarrollo de la Investigación –CODI– of Universidad de Antioquia. C.A.V.-T. is supported by Vicerrectoría de Investigaciones (UniValle) grant number 7859.



## REFERENCES

- L. A. Pachón and J. D. Sanabria-Gómez, *Classical and Quantum Gravity* **23**, 3251 (2006), arXiv:gr-qc/0603081.
- R. P. Kerr, *Physical Review Letters* **11**, 237 (1963).
- W. G. Laarakkers and E. Poisson, *Astrophys. J.* **512**, 282 (1999).
- V. S. Manko, J. Martín, and E. Ruiz, *Journal of Mathematical Physics* **36**, 3063 (1995).
- V. S. Manko, J. D. Sanabria-Gómez, and O. V. Manko, *Phys. Rev. D* **62**, 044048 (2000).
- H. Stephani, D. Kramer, M. MacCallum, C. Hoenselaers, and E. Herlt, *Exact solutions of Einstein's field equations*, 2nd ed. by Hans Stephani, Dietrich Kramer, Malcolm MacCallum, Cornelius Hoenselaers, and Eduard Herlt. Cambridge monographs on mathematical physics. Cambridge, UK: Cambridge University Press, 2003, edited by Stephani, H., Kramer, D., MacCallum, M., Hoenselaers, C., & Herlt, E. (2003).
- M. Stute and M. Camenzind, *Mon. Not. Roy. Astr. Soc.* **336**, 831 (2002), arXiv:astro-ph/0301466.
- E. Berti and N. Stergioulas, *Mon. Not. Roy. Astr. Soc.* **350**, 1416 (2004), arXiv:gr-qc/0310061.
- L. A. Pachón, J. A. Rueda, and J. D. Sanabria-Gómez, *Phys. Rev. D* **73**, 104038 (2006), arXiv:gr-qc/0606060.
- N. R. Sibgatullin and R. A. Sunyaev, *Astronomy Letters* **24**, 774 (1998), arXiv:astro-ph/9811028.
- G. B. Cook, S. L. Shapiro, and S. A. Teukolsky, *Astrophys. J.* **424**, 823 (1994).
- A. Tomimatsu and H. Sato, *Physical Review Letters* **29**, 1344 (1972).
- F. L. Dubeibe, L. A. Pachón, and J. D. Sanabria-Gómez, *Phys. Rev. D* **75**, 023008 (2007), arXiv:gr-qc/0701065.
- L. Stella and M. Vietri, *Astrophys. J. Lett.* **492**, L59+ (1998), arXiv:astro-ph/9709085.
- S. M. Morsink and L. Stella, *Astrophys. J.* **513**, 827 (1999), arXiv:astro-ph/9808227.
- L. Stella, M. Vietri, and S. M. Morsink, *Astrophys. J. Lett.* **524**, L63 (1999), arXiv:astro-ph/9907346.
- L. Stella and M. Vietri, *Physical Review Letters* **82**, 17 (1999), arXiv:astro-ph/9812124.
- Y.-F. Lin, M. Boutelier, D. Barret, and S.-N. Zhang, *Astrophys. J.* **726**, 74 (2011), arXiv:1010.6198 [astro-ph.HE].
- T. Johannsen and D. Psaltis, *Astrophys. J.* **726**, 11 (2011), arXiv:1010.1000 [astro-ph.HE].
- G. Török, P. Bakala, E. Šrámková, Z. Stuchlík, and M. Urbanec, *Astrophys. J.* **714**, 748 (2010), arXiv:1008.0088 [astro-ph.HE].
- F. D. Ryan, *Phys. Rev. D* **52**, 5707 (1995).
- A. Papapetrou, *Annalen der Physik* **447**, 309 (1953).
- F. J. Ernst, *Physical Review* **167**, 1175 (1968a).
- F. J. Ernst, *Physical Review* **172**, 1850 (1968b).
- N. R. Sibgatullin and N. M. Queen, *Oscillations and Waves in Strong Gravitational and Electromagnetic Fields*, XIV, 362 pp. 26 figs.. Springer-Verlag Berlin Heidelberg New York. Also Texts and Monographs in Physics, edited by Sibgatullin, N. R. & Queen, N. M. (1991).
- V. S. Manko and N. R. Sibgatullin, *Classical and Quantum Gravity* **10**, 1383 (1993).
- C. Hoenselaers and Z. Perjés, *Classical and Quantum Gravity* **7**, 1819 (1990).
- E. Ruiz, V. S. Manko, and J. Martín, *Phys. Rev. D* **51**, 4192 (1995).
- N. Bretón, V. S. Manko, and J. Aguilar Sánchez, *Classical and Quantum Gravity* **16**, 3725 (1999).
- P. Bakala, E. Šrámková, Z. Stuchlík, and G. Török, *Classical and Quantum Gravity* **27**, 045001 (2010).
- J. D. Sanabria-Gómez, J. L. Hernández-Pastora, and F. L. Dubeibe, *Phys. Rev. D* **82**, 124014 (2010), arXiv:1009.0320 [gr-qc].
- L. Herrera, G. A. González, L. A. Pachón, and J. A. Rueda, *Classical and Quantum Gravity* **23**, 2395 (2006).
- D. M. Lucchesi and R. Peron, *Physical Review Letters* **105**, 231103 (2010).
- N. R. Sibgatullin, *Astronomy Letters* **28**, 83 (2002), arXiv:astro-ph/0201155.
- N. Stergioulas, *Living Reviews in Relativity* **6**, 3 (2003), arXiv:gr-qc/0302034.
- P. Haensel, J. L. Zdunik, M. Bejger, and J. M. Lattimer, *Astron. Astrophys.* **502**, 605 (2009), arXiv:0901.1268 [astro-ph.SR].
- J.-F. Donati, I. D. Howarth, M. M. Jardine, P. Petit, C. Catala, J. D. Landstreet, J.-C. Bouret, E. Alecian, J. R. Barnes, T. Forveille, F. Paletou, and N. Manset, *Mon. Not. Roy. Astr. Soc.* **370**, 629 (2006), arXiv:astro-ph/0606156.

## APPENDIX

## METRIC FUNCTIONS

The functions  $A$ ,  $B$ ,  $C$ ,  $H$ ,  $G$ ,  $K$ , and  $I$  used to express the metric functions (17) are given by

$$A = \sum_{1 \leq i < j < k \leq 6} a_{ijk} r_i r_j r_k, \quad B = \sum_{1 \leq i < j \leq 6} b_{ij} r_i r_j, \quad C = \sum_{1 \leq i < j \leq 6} c_{ij} r_i r_j, \quad K = \sum_{1 \leq i < j < k \leq 6} a_{ijk}, \quad (\text{A1})$$

$$H = zA - (\beta_1 + \beta_2 + \beta_3)B + \sum_{1 \leq i < j < k \leq 6} h_{ijk} r_i r_j r_k + \sum_{1 \leq i < j \leq 6} (\alpha_i + \alpha_j) b_{ij} r_i r_j, \quad (\text{A2})$$

$$G = -(\beta_1 + \beta_2 + \beta_3)A + zB + \sum_{1 \leq i < j \leq 6} g_{ij} r_i r_j + \sum_{1 \leq i < j < k \leq 6} (\alpha_i + \alpha_j + \alpha_k) a_{ijk} r_i r_j r_k, \quad (\text{A3})$$

$$I = (f_1 + f_2 + f_3)(A - B) + (\beta_1 + \beta_2 + \beta_3 - z)C + \sum_{1 \leq i < j < k \leq 6} p_{ijk} r_i r_j r_k + \sum_{i=1}^6 p_i r_i + \sum_{1 \leq i < j \leq 6} [p_{ij} - (\alpha_i + \alpha_j) c_{ij}] r_i r_j, \quad (\text{A4})$$

with

$$\begin{aligned} r_i &= \sqrt{\rho^2 + (z - \alpha_i)^2}, \quad a_{ijk} = (-1)^{i+j+1} \Lambda_{ijk} \Gamma_{lmn}, \quad b_{ij} = (-1)^{i+j} \lambda_{ij} H_{lmnp}, \\ c_{ij} &= (-1)^{i+j} \lambda_{ij} [f(\alpha_l) \Gamma_{mnp} - f(\alpha_m) \Gamma_{npl} + f(\alpha_n) \Gamma_{plm} - f(\alpha_p) \Gamma_{lmn}], \\ h_{ijk} &= (-1)^{i+j+k} \Lambda_{ijk} (e_1^* \delta_{23|lmn} + e_2^* \delta_{31|lmn} + e_3^* \delta_{12|lmn}), \quad g_{ij} = (-1)^{i+j} \lambda_{ij} (\alpha_l \Gamma_{mnp} - \alpha_m \Gamma_{npl} + \alpha_n \Gamma_{plm} - \alpha_p \Gamma_{lmn}), \\ p_i &= (-1)^i D_i [f(\alpha_l) H_{mnp} - f(\alpha_m) H_{npsl} + f(\alpha_n) H_{plsm} - f(\alpha_p) H_{slmn} + f(\alpha_s) H_{lmnp}], \\ p_{ij} &= (-1)^{i+j} \lambda_{ij} (e_1^* \Upsilon_{23|lmnp} + e_2^* \Upsilon_{31|lmnp} + e_3^* \Upsilon_{12|lmnp}), \quad p_{ijk} = (-1)^{i+j+1} \Lambda_{ijk} (e_1^* \Psi_{23|lmn} + e_2^* \Psi_{31|lmn} + e_3^* \Psi_{12|lmn}), \\ \lambda_{ij} &= (\alpha_i - \alpha_j) D_i D_j, \quad \Lambda_{ijk} = (\alpha_i - \alpha_j)(\alpha_i - \alpha_k)(\alpha_j - \alpha_k) D_i D_j D_k, \\ D_i &= \frac{1}{(\alpha_i - \beta_1)(\alpha_i - \beta_2)(\alpha_i - \beta_3)}, \quad \Gamma_{lmn} = H_3(\alpha_l) \Delta_{12|mn} + H_3(\alpha_m) \Delta_{12|nl} + H_3(\alpha_n) \Delta_{12|lm}, \end{aligned}$$

and

$$\begin{aligned}\Delta_{lm|np} &= H_l(\alpha_n) H_m(\alpha_p) - H_l(\alpha_p) H_m(\alpha_n), \quad H_l(\alpha_n) = \frac{2 \prod_{p \neq n} (\alpha_p - \beta_l^*)}{\prod_{k \neq l}^3 (\beta_l^* - \beta_k^*) \prod_{k=1}^3 (\beta_l^* - \beta_k)} - \sum_{k=1}^3 \frac{2f_l^* f_k}{(\beta_l^* - \beta_k)(\alpha_n - \beta_k)}, \\ \delta_{lm|nps} &= \Delta_{lm|np} + \Delta_{lm|ps} + \Delta_{lm|sn}, \quad h_{l|mp} = H_3(\alpha_l) \delta_{12|mp}, \quad H_{l|mp} = h_{l|mp} + h_{m|npl} + h_{n|plm} + h_{p|lmn}, \\ \Psi_{lm|nps} &= f(\alpha_n) \Delta_{lm|ps} + f(\alpha_p) \Delta_{lm|sn} + f(\alpha_s) \Delta_{lm|np}, \\ \Upsilon_{lm|nprs} &= f(\alpha_n) \delta_{lm|prs} - f(\alpha_p) \delta_{lm|rsn} + f(\alpha_r) \delta_{lm|snp} - f(\alpha_s) \delta_{lm|npr},\end{aligned}$$

being  $\alpha$ 's the roots of the Sibgatullin equation [Sibgatullin and Queen \(1991\)](#); [Manko and Sibgatullin \(1993\)](#)

$$e(z) + \tilde{e}(z) + 2\tilde{f}(z)f(z) = 0. \quad (\text{A5})$$

#### KERR'S METRIC IN WEYL-PAPAPETROU QUASI-CYLINDRICAL COORDINATES

In order to keep comparisons in the save place, we consider useful to display the Kerr solution in the Weyl-Papapetrou quasi-cylindrical coordinates. For this case,

$$f = \frac{A\bar{A} - B\bar{B}}{(A - B)(\bar{A} - \bar{B})}, \quad e^{2\gamma} = \frac{A\bar{A} - B\bar{B}}{K\bar{K} \prod_{n=1}^2 r_n}, \quad \omega = \frac{\text{Im}[(A + B)\bar{H} - (\bar{A} + \bar{B})G]}{A\bar{A} - B\bar{B}}, \quad (\text{B1})$$

where for our own convenience we do not present the definition of each term, but present the final combination of them, i.e.,

$$\begin{aligned}A\bar{A} - B\bar{B} &= -8(a^2 - m^2)^3 (\rho^2 + z^2) \left( m^2 \sqrt{-2z\sqrt{m^2 - a^2} - a^2 + m^2 + \rho^2 + z^2} \sqrt{(\sqrt{m^2 - a^2} + z)^2 + \rho^2} \right. \\ &\quad \left. - 2a^2 \sqrt{-2z\sqrt{m^2 - a^2} - a^2 + m^2 + \rho^2 + z^2} \sqrt{(\sqrt{m^2 - a^2} + z)^2 + \rho^2 + a^2 m^2 - m^4 + m^2 \rho^2 + m^2 z^2} \right),\end{aligned} \quad (\text{B2})$$

$$\begin{aligned}(A - B)(\bar{A} - \bar{B}) &= -8(m^2 - a^2)^3 \\ &\quad \times (\rho^2 + z^2) \left( a^2 \left( 2m \left( \sqrt{-2z\sqrt{m^2 - a^2} - a^2 + m^2 + \rho^2 + z^2} + \sqrt{2z\sqrt{m^2 - a^2} - a^2 + m^2 + \rho^2 + z^2} \right) \right. \right. \\ &\quad \left. \left. + 2\sqrt{-2z\sqrt{m^2 - a^2} - a^2 + m^2 + \rho^2 + z^2} \sqrt{2z\sqrt{m^2 - a^2} - a^2 + m^2 + \rho^2 + z^2} + 3m^2 \right) \right. \\ &\quad \left. - m^2 \left( 2m \left( \sqrt{-2z\sqrt{m^2 - a^2} - a^2 + m^2 + \rho^2 + z^2} + \sqrt{2z\sqrt{m^2 - a^2} - a^2 + m^2 + \rho^2 + z^2} \right) \right. \right. \\ &\quad \left. \left. + \sqrt{-2z\sqrt{m^2 - a^2} - a^2 + m^2 + \rho^2 + z^2} \sqrt{2z\sqrt{m^2 - a^2} - a^2 + m^2 + \rho^2 + z^2} + 3m^2 + \rho^2 + z^2 \right) \right),\end{aligned} \quad (\text{B3})$$

$$K\bar{K} \prod_{n=1}^2 r_n = 16(m^2 - a^2)^4 (\rho^2 + z^2) \sqrt{(z - \sqrt{m^2 - a^2})^2 + \rho^2} \sqrt{(\sqrt{m^2 - a^2} + z)^2 + \rho^2} \quad (\text{B4})$$

$$\begin{aligned}\text{Im}[(A + B)\bar{H} - (\bar{A} + \bar{B})G] &= 16am(m^2 - a^2)^3 (\rho^2 + z^2) \left( -m^2 \sqrt{-2z\sqrt{m^2 - a^2} - a^2 + m^2 + \rho^2 + z^2} \right. \\ &\quad \left. - m \sqrt{-2z\sqrt{m^2 - a^2} - a^2 + m^2 + \rho^2 + z^2} \sqrt{(\sqrt{m^2 - a^2} + z)^2 + \rho^2} \right. \\ &\quad \left. + a^2 \sqrt{-2z\sqrt{m^2 - a^2} - a^2 + m^2 + \rho^2 + z^2} - z \sqrt{m^2 - a^2} \sqrt{-2z\sqrt{m^2 - a^2} - a^2 + m^2 + \rho^2 + z^2} \right. \\ &\quad \left. - m^2 \sqrt{(\sqrt{m^2 - a^2} + z)^2 + \rho^2} + a^2 \sqrt{(\sqrt{m^2 - a^2} + z)^2 + \rho^2} \right. \\ &\quad \left. + z \sqrt{m^2 - a^2} \sqrt{(\sqrt{m^2 - a^2} + z)^2 + \rho^2} + a^2 m - m^3 + m\rho^2 + m^2 z^2 \right).\end{aligned} \quad (\text{B5})$$

From here, it is clear how changing  $a \rightarrow -a$  will cause only a global change in the sign of the metric function  $\omega$  and therefore only a change in the  $g_{t\phi}$  metric component.